IEEE Access
Multidisciplinary | Rapid Review | Open Access Journal

Received 16 March 2023, accepted 1 April 2023, date of publication 5 April 2023, date of current version 11 April 2023.

Digital Object Identifier 10.1109/ACCESS.2023.3264968

RESEARCH ARTICLE

Advancements in 2D/3D Image Registration Methods

FAWAZ HJOUJ[1], MOHAMED SOUFIANE JOUINI[1], AND MOHAMMAD AL-KHALEEL[1,2]
[1]Department of Mathematics, Khalifa University, Abu Dhabi, United Arab Emirates
[2]Department of Mathematics, Yarmouk University, Irbid 21163, Jordan

Corresponding author: Fawaz Hjouj (fawaz.hjouj@ku.ac.ae)

ABSTRACT In this paper, we present methods for identifying an image from a given set of Radon projections. Given a suitably regular 2-D or 3-D function, we form a new function g from f using a linear transformation. We show how the Radon projections of f and g can be used to determine the transformation. The proposed algorithms introduce three major contributions: 1) Improvements on the 2-D setting using the moments of the Radon projections with only two orthogonal projections. 2) A natural extension of the 2-D setting to work with the 3-D setting. In particular, reducing the 3-D problem to a 2-D problem so that we can recover a translation, a scaling, or a rotation transformation of a 3-D object in the Radon domain. 3) An efficient method of recovering a rotation of a 3-D image around an arbitrary axis and an angle of rotation.

INDEX TERMS Digital watermarking, affine transformation, radon transform, linear transformation.

I. INTRODUCTION

One of the key imaging technologies is image registration, which matches two or more images. Image registration establishes correspondences between different images showing diverse views of objects or organs. These images might have been taken at various points in time, from various angles, from different devices or perspectives, or even reveal various kinds of information. Many applications, including medical image analysis, recognition, and industrial vision, use image registration. Interestingly, there is a large number of application areas demanding for image registration, and image registration has impact on basically every imaging technique [1], [2], [3], [4], [5].

Specific examples include change detection and motion correction, data fusion, spatial normalization of data, stitching (generating a global picture from partial views), template matching and identification, studying an inspected image, or comparing current images with a data base. Moreover, imaging modalities such as diffusion tensor imaging rely on image registration. Therefore, image registration is an important computational tool.

The associate editor coordinating the review of this manuscript and approving it for publication was Abdel-Hamid Soliman.

Geometric transformation of an image might be classified into two main types: linear and nonlinear transformation. Linear transformation, which is the main subject of this paper, includes rotation, reflection, dilation, and many other classical linear transformations.

Over the past decades, various image registration methods have been proposed. Among the existing methods, the transform-based method [6], [7], [8], [9], [10], [11], [12], [13], [14], [15], [16], [17], [18], [19], [20], [21], [22], feature-based method [23], [24], and others. The term ''transform-based methods'' is used here in a global sense. This includes the Radon and Fourier transform, Trace transform, and others. Within this approach, we find different algorithms that are based on different implementations such as the methods of moments of the projections, correlations, the combination of log-polar transform and 1D phase-only correlation. The method of moments, like Zernike moments [12] and Krawtchouk moments [13], is frequently used; in fact, many shape descriptors that are commonly used in the literature are based on Radon transform, including complex moments as in [14], Zernike moments as in [15] and many others. Direct implementation in Radon domain is presented in [6], [7], and [8]. The Fourier phase matching method [9] is applied on the registration of radiography and computed tomography projections. In [10] the authors use the results obtained in [6]

to identify the transform parameters for a fast-matching algorithm. Another major approach related to Radon transform uses invariant pattern recognition, [16], [17], [18].

A common approach to estimate the image rotation, is to convert the rotation into a geometrical translation and estimate the translation. For example, [17] defines the R-transform or signature so that a rotation of the image by an angle θ implies a translation of the R-transform by θ. Another example is the combination of log-polar transform and 1D phase-only correlation [21], [22]. Similarly, the authors of [10] proposed the rotation estimation algorithm based on Radon transform. This method converts the rotation into the geometrical shift and estimate the shift by the phase correlation method which is robust to noise. However, the precision of the phase correlation method is limited to integer precision.

In the 2D/3D image registration we are interested in finding the optimal geometric transformation that aligns a distorted image to a reference image. In doing so, we work with the 2-D observations that will eventually allow us to work with one dimensional data. A review of 2D/3D image registration methods is given [25], [26]. For example, in [26] the authors propose a 2D/3D image registration method based on evaluation of similarity between corresponding 3-D and 2-D gradient covariances using backprojection. In [27], the Radon transform of the reference image and the images to be matched is calculated first, then a certain Fourier invariant descriptor for each 1-D projection image is computed. Authors of [28] suggest an intensity-driven 2D/3D multiresolution registration approach using the normalized gradient fields distance measure. Reference [29] introduces a 2D/3D medical image registration algorithm based on normalized cross-correlation.

In this paper, we present methods for recovering a transformation that relates a 2-D or 3-D input distorted image to a known reference image. To some degree, this work is an extension and improvement of an existing algorithms, [6], [7]. In [6], the authors addressed the problems of shifting, rotating, reflecting, dilating, and translating between a reference image and a distorted image. The general form of the problem is presented in [7] where the matrix of the transformation is recovered through its singular value decomposition. The current proposed algorithms introduce the following contributions:

1) For the 2-D setting: we propose a solution to the non-uniform scaling problem and we give an alternative solution to the rotation problem using only two orthogonal projections such as the view angles 0 and $\pi/2$.

2) For the 3-D setting: we propose a procedure to reduce the 3-D to 2-D calculations and use it to compute the centroid and the scaling parameters. In addition, we devise an efficient method of recovering a rotation of a 3-D image around an arbitrary axis and an angle of rotation.

Our work is organized as follows: in section II, a background material is presented, this includes, the Radon transforms, the projection's moments, and the linear transformation of images. In section III, the theoretical work for the 2D/3D problem is presented. Section IV presents validation and results discussion. Finally, our conclusion is provided in section V.

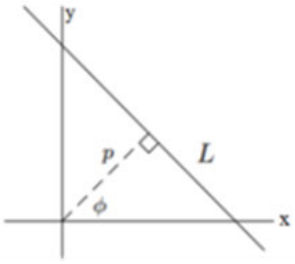

FIGURE 1. The line L from (2) specified by the coordinates (p, φ).

II. BACKGROUND MATERIAL

This section presents a review of three mathematical tools and notation that will be used in this work. These tools are: the Radon transform, the projection's moments, and the linear transformation of images. Let (x, y) designate the coordinates of points in the plane and let f be a suitably regular real valued function on some domain D of R^2. Then, the two-dimensional Radon transform of f is the line integral along all possible lines L, given by

$$f^{\vee} = \int_L f\,(x, y)\,ds \tag{1}$$

As shown in Fig1, the line L depends on the values p and φ and is described by the equation

$$x\,cos\varphi + y\,sin\varphi = p \tag{2}$$

It is convenient to write

$$f_{\varphi}^{\vee}(p) = \int_{-\infty}^{\infty} f(p\cos\varphi - t\,sin\,\varphi, p\,sin\,\varphi + t\,cos\,\varphi)dt \tag{3}$$

Using vector notation, let $\boldsymbol{\xi} =< cos\varphi, sin\varphi >$ be a unit vector and let $\boldsymbol{x} =< x, y >$ be a vector with components x and y, then $f(\boldsymbol{x})$ means $f(x, y)$. In this way, the line L is described by $\boldsymbol{\xi}.\boldsymbol{x} = x\,cos\varphi + y\,sin\varphi = p$. Then, the transform is written as

$$f^{\vee}(p, \xi) = \iint_{R^2} f\,(\boldsymbol{x})\,\delta\,(p - \boldsymbol{\xi}.\boldsymbol{x})\;dx\,dy \tag{4}$$

δ is the Dirac function.

Similarly for the three dimensional setting, (with some changes of the notation); let $\boldsymbol{\xi} =< \xi_1, \xi_2, \xi_3 >$ be a unit vector and let $\boldsymbol{x} =< x, y, z >$ be a vector in R^3 with components x, y, z, and $d\boldsymbol{x} = dxdydz$. Let F be a three dimensional function. The equation

$\boldsymbol{\xi}.\boldsymbol{x} = \xi_1 x + \xi_2 y + \xi_3 z = q$ defines a plane, and the Radon transform of F is given by

$$F^{\vee}(q, \boldsymbol{\xi}) = \iiint_{R^3} F\,(\boldsymbol{x})\;\delta\;(q - \boldsymbol{\xi}.\boldsymbol{x})\;dxdydz \tag{5}$$

The integrations here are over planes rather than lines. Here, q is the perpendicular distance from the origin to the plane,

and $\boldsymbol{\xi}$ is a unit vector along q that defines the orientation of the plane. Radon showed that it is possible to recover a suitably regular real valued function from the set of all projections, [30], [31]. This transform found its applications in diverse fields including medical applications, digital rock physics, image processing, and others, see for instance [32], [33], [34], [35], [36], [37].

Another tool to review is the projection's moments. The n^{th} order moment of $f\ (x, y)$ is given by

$$M_{s,t}(f) = \int_{-\infty}^{\infty}\int_{-\infty}^{\infty} x^s y^t\, f(x, y)dxdy \tag{6}$$

where s, t are nonnegative integers with $s + t = n$.

The n^{th} moment of the projection $f_{\varphi}^{\vee}(p)$ is written as,

$$M_{\varphi}^{(n)}(f^{\vee}) := \int_{-\infty}^{\infty} p^n f_{\varphi}^{\vee}(p)dp, \quad n = 0, 1, 2, \ldots \varphi \in [0, \pi] \tag{7}$$

The following known result, [38], shows to what extent the moments of projections can determine the moments of the function (image):

$$M_{\varphi}^{(n)}(f) = \sum_{l=0}^{n} \binom{n}{l} cos^{n-l}(\varphi)\,.\,sin^{l}(\varphi) \cdot \iint_{-\infty-\infty}^{\infty\infty} x^{n-l}y^{l} f(x, y)dxdy \tag{8}$$

that can be written as,

$$M_{\varphi}^{(n)}(f^{\vee}) = \sum_{l=0}^{n} \binom{n}{l} cos^{n-l}(\varphi)\,.\,sin^{l}(\varphi)\,.M_{n-l,l}(f) \tag{9}$$

It is possible, using (9), to show that,

$$\begin{aligned} M_{\varphi}^{(1)}(f^{\vee}) &:= \int_{-\infty}^{\infty} pf^{\vee}(p, \varphi)\, dp \\ &= M_0^{(1)}(f^{\vee})cos\varphi + M_{\frac{\pi}{2}}^{(1)}(f^{\vee})sin\varphi \end{aligned} \tag{10}$$

This can be written as a cosine function,

$$\begin{aligned} M_{\varphi}^{(1)}(f^{\vee}) &= Rcos(\varphi + \alpha); \\ \mathrm{R} &= \sqrt{[M_0^{(1)}(f^{\vee})]^2 + [M_{\frac{\pi}{2}}^{(1)}(f^{\vee})\,]^2}, \text{ and} \\ tan(\alpha) &= \frac{M_0^{(1)}(f^{\vee})}{M_{\frac{\pi}{2}}^{(1)}(f^{\vee})} \end{aligned} \tag{11}$$

Finally, we review the Radon transform of a linear transformation which is presented in [20]. Let f be nonnegative 2-D function and let A be a nonsingular matrix. Consider the transformation

$$g(x, y) := f(A\boldsymbol{x}), \boldsymbol{x} = \begin{pmatrix} x \\ y \end{pmatrix} \tag{12}$$

Then,

$$g^{\vee}(p, \boldsymbol{\xi}) = \Delta f^{\vee}(p, B^T\boldsymbol{\xi}), \quad \text{where } \Delta = |\det(B)|,\ \mathrm{B} = A^{-1} \tag{13}$$

Similarly, for a 3-D function F and the transformation $G(x, y, z) := F(A\boldsymbol{x}), \boldsymbol{x} = \begin{pmatrix} x \\ y \\ z \end{pmatrix}$; we have

$$G^{\vee}(q, \boldsymbol{\xi}) = \Delta\, F^{\vee}(q, B^T\boldsymbol{\xi}) \tag{14}$$

Define, $\boldsymbol{\mu} = B^T\boldsymbol{\xi}$ and let the angles θ, φ such that $\boldsymbol{\xi} = \begin{pmatrix} \cos\theta \\ \sin\theta \end{pmatrix}$, and $\boldsymbol{\mu} = B^T\boldsymbol{\xi} = |\boldsymbol{\mu}| \begin{pmatrix} \cos\varphi \\ \sin\varphi \end{pmatrix}$

Then, (13), (14) are written as

$$g^{\vee}(p, \theta) = \frac{\Delta}{|\boldsymbol{\mu}|} f^{\vee}\left(\frac{p}{|\boldsymbol{\mu}|},\ \varphi\right) \tag{15}$$

$$G^{\vee}(q, \xi) = \frac{\Delta}{|\boldsymbol{\mu}|} F^{\vee}\left(\frac{q}{|\boldsymbol{\mu}|}, \frac{\boldsymbol{\mu}}{|\boldsymbol{\mu}|}\right) \tag{16}$$

Consider a reference image f and an inspected image g, where g is obtained from f by the linear transformation (12). One efficient way to obtain the matrix of transformation is through the singular value decomposition [7], [8]. However, that approach requires the Radon projections of all view angles. As said, the problems of shifting, uniform scaling, rotation, reflection transformations, and others are discussed in [6]. In particular, the centroid calculations are as follows:

$$\bar{x} = \frac{\int_{-\infty}^{\infty} p\, g^{\vee}(p, 0)\, dp}{\int_{-\infty}^{\infty} g^{\vee}(p, 0)\, dp}, \quad \text{and } \bar{y} = \frac{\int_{-\infty}^{\infty} p\, g^{\vee}\left(p, \frac{\pi}{2}\right) dp}{\int_{-\infty}^{\infty} g^{\vee}\left(p, \frac{\pi}{2}\right) dp} \tag{17}$$

III. METHODOLOGY

This section proposes new ideas for solving some transformation problems that include: the 2-D non-uniform scaling, the 2-D rotation, reducing the 3-D calculation to the 2-D setting, the 3-D scaling, the 3-D centroid, and some 3-D rotation problems. These ideas are presented in the following subsections.

A. THE 2-D SCALING PROBLEM

The 2-D uniform scaling problem was solved in [6]. Here, we consider the non-uniform scaling problem, based on only two view angles of projections.

Suppose that the function g is obtained from the function f by the matrix $\mathrm{A} = \begin{bmatrix} s_1 & 0 \\ 0 & s_2 \end{bmatrix}$, $s_1, s_2 > 0$ so that

$$g(x, y) = f(s_1x, s_2y) \tag{18}$$

Apply (15), using the angles 0 and $\frac{\pi}{2}$, we write,

$$g^{\vee}(p, 0) = \frac{1}{s_2} f^{\vee}(s_1p, 0), \text{ and} \tag{19}$$

$$g^{\vee}\left(p, \frac{\pi}{2}\right) = \frac{1}{s_1} f^{\vee}(s_2p, \frac{\pi}{2}) \tag{20}$$

Direct calculations show that,

$$\Delta = \frac{1}{s_1s_2} = \frac{\int_{-\infty}^{\infty} g^{\vee}(p, 0)\ dp}{\int_{-\infty}^{\infty} f^{\vee}(p, 0)\ dp} \tag{21}$$

and that

$$s_1 = \Delta . \frac{\int_{-\infty}^{\infty} [f^{\vee}\left(p, \frac{\pi}{2}\right)]^2}{\int_{-\infty}^{\infty} [g^{\vee}\left(p, \frac{\pi}{2}\right)]^2} dp,$$
$$s_2 = \Delta . \frac{\int_{-\infty}^{\infty} [f^{\vee}(p, 0)]^2}{\int_{-\infty}^{\infty} [g^{\vee}(p, 0)]^2} dp \tag{22}$$

Thus, using the angles 0 and $\frac{\pi}{2}$ we can apply (21) and (22) to compute the scaling parameters s_1 and s_2 that link g to f. For the case of a uniform scaling when $g(x, y) = f(sx, sy)$, it follows from (21) that

$$s = \sqrt{\frac{\int_{-\infty}^{\infty} f^{\vee}(p, 0)dp}{\int_{-\infty}^{\infty} g^{\vee}(p, 0)\, dp}} \tag{23}$$

B. THE 2-D ROTATION PROBLEM

Suppose that the function g is obtained from the function f by the real rotation parameter θ so that $A = \begin{bmatrix} \cos(\theta) & \sin(\theta) \\ -\sin(\theta) & \cos(\theta) \end{bmatrix}$, and

$$g(x, y) = f(xcos\theta + y\sin\theta, -xsin\theta + ycos\theta) \tag{24}$$

then, from (15) we have,

$$g^{\vee}(p, \varphi) = f^{\vee}(p, \varphi - \theta) \tag{25}$$

An efficient procedure for recovering the angle of rotation is introduced in [6]. But this method requires the Radon projections of the inspected image for all view angles.

In the following, we devise another approach that requires only two angles of projection. Let us apply (10) to both sides of (25):

$M_{\varphi}^{(1)}(g^{\vee}) = M_{\varphi-\theta}^{(1)}(f^{\vee})$, equivalently,

$$M_0^{(1)}(g^{\vee})\, cos\varphi + M_{\frac{\pi}{2}}^{(1)}(g^{\vee})\, sin\varphi = M_0^{(1)}(f^{\vee}) \cos(\varphi - \theta) + M_{\frac{\pi}{2}}^{(1)}(f^{\vee})\, sin(\varphi - \theta) \tag{26}$$

for any angle φ, Since each side of (26) is a cosine function as shown in (11), then the angle θ is simply the shift in equation (26). Thus, we can use (26) to compute the angle of rotation that links g to f. In this way, only two projections with angles $\varphi = 0, \frac{\pi}{2}$, are needed.

C. FROM 3-D TO 2-D

In certain parts of the discussion, we reduce the calculation to the 2-D transform. The following elementary observation is essential to this approach. Let $f(x, y)$ be a 2-D function. Then, for any φ we have,

$$\int_{-\infty}^{\infty}\int_{-\infty}^{\infty} f(x, y)dxdy = \int_{-\infty}^{\infty} f^{\vee}(p, \varphi)\, dp \tag{27}$$

In several instances of our calculations, we use the three vectors: $\boldsymbol{\xi} = \boldsymbol{i} =< 1, 0, 0 >$, $\boldsymbol{\xi} = \boldsymbol{j} =< 0, 1, 0 >$, or $\boldsymbol{\xi} = \boldsymbol{k} =< 0, 0, 1 >$.

Consider, for instance, the case $\boldsymbol{\xi} = \boldsymbol{k} =< 0, 0, 1 >$.

To compute $F^{\vee}(q, \boldsymbol{k})$, (which is an integration over the horizontal plane $z = q$); define:

$$f_{q,\boldsymbol{k}}^{\vee}(p, \varphi) = \int_{-\infty}^{\infty} F(p\cos\varphi - t\sin\varphi, p\sin\varphi + t\cos\varphi,\ q)\, dt \tag{28}$$

In other words, $f_{q,\boldsymbol{k}}^{\vee}(p, \varphi)$ means the two-dimensional line integral of $F(x, y, q)$ on the plane $z = q$, defined by p, φ that are given in (2-3). Using (27), it is then true that,

$$F^{\vee}(q, \boldsymbol{k}) = \int_{-\infty}^{\infty}\int_{-\infty}^{\infty} F(x, y, q)dxdy = \int_{-\infty}^{\infty} f_{q,\boldsymbol{k}}^{\vee}(p, \varphi)\, dp,$$

for any φ. In particular,

$$F^{\vee}(q, \boldsymbol{k}) = \int_{-\infty}^{\infty}\int_{-\infty}^{\infty} F(x, y, q)dxdy = \int_{-\infty}^{\infty} f_{q,\boldsymbol{k}}^{\vee}(p, 0)\, dp \tag{29}$$

Similarly,

$$F^{\vee}(q, \boldsymbol{j}) = \int_{-\infty}^{\infty}\int_{-\infty}^{\infty} F(x, q, z)\, dxdz = \int_{-\infty}^{\infty} f_{q,\boldsymbol{j}}^{\vee}(p, \varphi)\, dp,$$

where the values p and φ are seated in the $xz-$ plane. In particular,

$$F^{\vee}(q, \boldsymbol{j}) = \int_{-\infty}^{\infty}\int_{-\infty}^{\infty} F(x, q, z)dxdz = \int_{-\infty}^{\infty} f_{q,\boldsymbol{j}}^{\vee}(p, 0)\, dp \tag{30}$$

and,

$$F^{\vee}(q, \boldsymbol{i}) = \int_{-\infty}^{\infty}\int_{-\infty}^{\infty} F(q, y, z)dydz = \int_{-\infty}^{\infty} f_{q,\boldsymbol{i}}^{\vee}(p, \varphi)\, dp,$$

values p and φ are seated in the $yz-$ plane. In particular,

$$F^{\vee}(q, \boldsymbol{i}) = \int_{-\infty}^{\infty}\int_{-\infty}^{\infty} F(x, q, z)\, dxdz = \int_{-\infty}^{\infty} f_{q,\boldsymbol{i}}^{\vee}(p, 0)\, dp \tag{31}$$

D. THE CENTROID OF F

Let $(\overline{x}, \overline{y}, \overline{z})$ be the center of mass of the function F in the domain E. With arguments similar to (17), we determine this point. Observe that,

$$\overline{x}\frac{\int_{-\infty}^{\infty}\int_{-\infty}^{\infty}\int_{-\infty}^{\infty} x\, F(x, y, z)dxdydz}{\int_{-\infty}^{\infty}\int_{-\infty}^{\infty}\int_{-\infty}^{\infty} F(x, y, z)dxdydz} = \frac{\int_{-\infty}^{\infty} x\, F^{\vee}(x, \boldsymbol{i})\, dx}{\int_{-\infty}^{\infty} F^{\vee}(x, \boldsymbol{i})\, dx} \tag{32}$$

Similarly, for $\bar{y}$ and $\bar{z}$ so we can write,

$$\bar{x} = \frac{\int_{-\infty}^{\infty} qF^{\vee}(q,\boldsymbol{i})dq}{\int_{-\infty}^{\infty} F^{\vee}(q,\boldsymbol{i})dq}$$
$$\bar{y} = \frac{\int_{-\infty}^{\infty} qF^{\vee}(q,\boldsymbol{j})dq}{\int_{-\infty}^{\infty} F^{\vee}(q,\boldsymbol{j})dq}$$
$$\bar{z} = \frac{\int_{-\infty}^{\infty} qF^{\vee}(q,\boldsymbol{k})dq}{\int_{-\infty}^{\infty} F^{\vee}(q,\boldsymbol{k})dq} \tag{33}$$

E. THE 3-D SCALING PROBLEM

Suppose that the function G is obtained from the function F by the matrix of transformation $A = \begin{bmatrix} s_1 & 0 & 0 \\ 0 & s_2 & 0 \\ 0 & 0 & s_3 \end{bmatrix}$, $s_1, s_2, s_3 > 0$ so that

$$G(x,y,z) = F(s_1x, s_2y, s_3z) \tag{34}$$

Apply (16), with the vectors $\boldsymbol{i},\boldsymbol{j},\boldsymbol{k}$,

$$G^{\vee}(q,\boldsymbol{i}) = \frac{1}{s_2s_3} F^{\vee}(s_1q,\boldsymbol{i})$$
$$G^{\vee}(q,\boldsymbol{j}) = \frac{1}{s_1s_3} F^{\vee}(s_2q,\boldsymbol{j})$$
$$G^{\vee}(q,\boldsymbol{k}) = \frac{1}{s_1s_2} F^{\vee}(s_3q,\boldsymbol{k}) \tag{35}$$

Using any of the three equations of (35), we write

$$\Delta = \frac{1}{s_1s_2s_3} = \frac{\int_{-\infty}^{\infty} G^{\vee}(q,\boldsymbol{k})\ dq}{\int_{-\infty}^{\infty} F^{\vee}(q,\boldsymbol{k})\ dq} \tag{36}$$

If each of the three equations of (35) is squared and integrated with respect to q, we obtain the following,

$$s_2s_3 = \Delta \cdot \frac{\int_{-\infty}^{\infty} [F^{\vee}(q,\boldsymbol{i})\ ]^2\ dq}{\int_{-\infty}^{\infty} [G^{\vee}(q,\boldsymbol{i})\ ]^2\ dq}$$
$$s_1s_3 = \Delta \cdot \frac{\int_{-\infty}^{\infty} [F^{\vee}(q,\boldsymbol{j})\ ]^2\ dq}{\int_{-\infty}^{\infty} [G^{\vee}(q,\boldsymbol{j})\ ]^2\ dq}$$
$$s_1s_2 = \Delta \cdot \frac{\int_{-\infty}^{\infty} [F^{\vee}(q,\boldsymbol{k})\ ]^2\ dq}{\int_{-\infty}^{\infty} [G^{\vee}(q,\boldsymbol{k})\ ]^2\ dq} \tag{37}$$

Thus, (36-37) determine the scaling parameters $s_1, s_2,$ and s_3 that link G to F. A special case occurs when $s_1 = s_2 = s_3 = s$. Then, from (36) we have

$$s = \sqrt[3]{\frac{\int_{-\infty}^{\infty} F^{\vee}(q,\boldsymbol{k})\ dq}{\int_{-\infty}^{\infty} G^{\vee}(q,\boldsymbol{k})\ dq}} \tag{38}$$

F. 3-D ROTATION ABOUT THE Z- AXIS

Suppose, for instance, that the function G is obtained from the function F by the real rotation parameter θ about the $z-$ axis using the matrix, $A = \begin{bmatrix} \cos(\theta) & \sin(\theta) & 0 \\ -\sin(\theta) & \cos(\theta) & 0 \\ 0 & 0 & 1 \end{bmatrix}$, so that

$$G(x,y,z) = F(xcos\theta + ysin\theta, -xsin\theta + ycos\theta,\ z) \tag{39}$$

We may reduce the problem of finding the angle θ by considering the rotation of the $xy-$ planes of both F and G. In this way, we work with $f^{\vee}_{0,\boldsymbol{k}}(p,\varphi)$ and $g^{\vee}_{0,\boldsymbol{k}}(p,\varphi)$ from (28). If we choose to apply (26), then θ is the shift parameter of the equation:

$$M_0^{(1)}\left[g^{\vee}_{0,k}\right] cos\varphi + M_{\frac{\pi}{2}}^{(1)}\left[g^{\vee}_{0,k}\right] sin\varphi$$
$$= M_0^{(1)}[f^{\vee}_{0,k}]\cos(\varphi-\theta) + M_{\frac{\pi}{2}}^{(1)}[f^{\vee}_{0,k}] sin(\varphi-\theta) \tag{40}$$

Similar arguments can be performed for the rotation about the x or the $y-$ axis.

G. 3-D ROTATION ABOUT AN ARBITRARY AXIS WITH ARBITRARY ANGLE OF ROTATION

The matrix of a proper rotation by angle θ around an axis specified by the unit vector $\boldsymbol{u} = < a, b, c >$ is given by (41), as shown at the bottom of the page. Suppose that the function G is obtained from the function F such that

$$G(\boldsymbol{x}) := F(A_{\boldsymbol{u},\theta}\boldsymbol{x}); \quad \boldsymbol{x} = \begin{pmatrix} x \\ y \\ z \end{pmatrix} \tag{42}$$

Apply (14), we have

$$G^{\vee}(q,\boldsymbol{\xi}) = F^{\vee}(q, A_{\boldsymbol{u},\theta}\boldsymbol{\xi}) \tag{43}$$

In view of these considerations, consider the upper half of the unit sphere

$$\mathcal{U} = \{\boldsymbol{u} = < a, b, c >,\ a^2 + b^2 + c^2 = 1,$$
$$-1 \le a, b \le 1,\ \text{and}\ 0 \le z \le 1\} \tag{44}$$

and the space of unit vectors

$$\boldsymbol{\xi} = \{(sin\Phi\ cos\Theta, sin\Phi\ sin\Theta, cos\Phi),$$
$$0 \le \Phi < \pi, 0 \le \Theta < 2\pi\} \tag{45}$$

Define the objective function,

$$\Psi(\boldsymbol{u},\theta) = \int_{\boldsymbol{\xi}} [\int_{-\infty}^{\infty} \left|G^{\vee}(q,\boldsymbol{\xi}) - F^{\vee}\left(q, A_{\boldsymbol{u},\theta}\xi\right)\right|\ dq\ ]d\boldsymbol{\xi} \tag{46}$$

$$A_{\boldsymbol{u},\theta} = \begin{bmatrix} \cos\theta + a^2(1-cos\theta) & ab(1-cos\theta) - csin\theta & ac(1-cos\theta) + bsin\theta \\ ab(1-cos\theta) + csin\theta & \cos\theta + b^2(1-cos\theta) & bc(1-cos\theta) - asin\theta \\ ac(1-cos\theta) - bsin\theta & bc(1-cos\theta) + asin\theta & \cos\theta + c^2(1-cos\theta) \end{bmatrix} \tag{41}$$

The integral $d\boldsymbol{\xi}$ is with respect to the 3-dimensional Lebesgue measure. We will numerically find $\boldsymbol{u}\in\mathcal{U}$, and $0 \leq \theta < 2\pi$ that minimize (46), from which, both axis and angle of rotation are determined.

IV. DISCUSSION

We present our discussion through the following examples.

A. EXAMPLE 1: A VALIDATION EXAMPLE

Consider the function $F(x, y, z) = 1$ on the region $E = \{(x, y, z) : 2 \leq x \leq 4,\ 2 \leq y \leq 4, 0 \leq z \leq 2\}$, shown in Fig 2a. A typical horizontal slice of this function would be equivalent to the image in Fig 2b, in the $xy-$ plane. Consider (28) and (29); we calculate the following:

$F^{\vee}(q, \boldsymbol{k}) = \int_2^4 f^{\vee}_{\boldsymbol{q},\boldsymbol{k}}(p, 0)\, dp = 4$,(Area of the box in Fig 2b), for any $0 \leq q \leq 2$. Fig 2c shows the graph of $F^{\vee}(q, \boldsymbol{k})$, and Fig 2d shows the graph of $F^{\vee}(q, \boldsymbol{i})$, which is in this example, the same for $F^{\vee}(q, \boldsymbol{j})$. Apply (33), we see that, $\bar{x} = \frac{\int_{-\infty}^{\infty} qF^{\vee}(q,i)dq}{\int_{-\infty}^{\infty} F^{\vee}(q,i)dq} = \frac{24}{8} = 3 = \bar{y} = \frac{\int_{-\infty}^{\infty} qF^{\vee}(q,j)dq}{\int_{-\infty}^{\infty} F^{\vee}(q,j)dq}$ and $\bar{z} = \frac{\int_{-\infty}^{\infty} qF^{\vee}(q,k)dq}{\int_{-\infty}^{\infty} F^{\vee}(q,k)dq} = \frac{8}{8} = 1$.

Assume now that F is subjected to a scaling transformation so that G from (34) is given by $G(x, y, z) = F(4x, 2y, 1z)$ that is shown in Fig 3.

A slice of Fig 3 parallel to the $yz-$ plane together with the profile $G^{\vee}(q, \boldsymbol{i})$ are shown in Fig 4a-b. A slice of Fig 3 parallel to the $xz-$ plane together with the profile $G^{\vee}(q, \boldsymbol{j})$ are shown in Fig 4c-d; and a slice of Fig 3 parallel to the $xy-$ plane with the profile $G^{\vee}(q, \boldsymbol{k})$ are shown in Fig 4e-f.

In view of (36-37) we find,

$$\boldsymbol{\Delta} = \frac{1}{\boldsymbol{s_1 s_2 s_3}} = \frac{\int_0^2 \boldsymbol{G^{\vee}(q, k)\, dq}}{\int_2^4 \boldsymbol{F^{\vee}(q, k)\, dq}} = \frac{1}{8}$$

$$s_2 s_3 = \Delta . \frac{\int_2^4 [F^{\vee}(q, \boldsymbol{i})]^2\, dq}{\int_5^1 [G^{\vee}(q, \boldsymbol{i})]^2\, dq} = \frac{1}{8} . \frac{32}{2} = 2$$

$$s_1 s_3 = \Delta . \frac{\int_2^4 [F^{\vee}(q, \boldsymbol{j})]^2\, dq}{\int_1^2 [G^{\vee}(q, \boldsymbol{j})]^2\, dq} = \frac{1}{8} . \frac{32}{1} = 4$$

$$s_1 s_2 = \Delta . \frac{\int_{-\infty}^{\infty} [F^{\vee}(q, \boldsymbol{k})]^2\, dq}{\int_{-\infty}^{\infty} [G^{\vee}(q, \boldsymbol{k})]^2\, dq} = \frac{1}{8} . \frac{32}{\frac{1}{2}} = 8$$

B. EXAMPLE 2: A 3-D ROTATION ABOUT THE z - AXIS

Suppose that the function $F(x, y, z) = 1$ on the region A, shown in Fig 5a, and that G in Fig 5b is obtained from F by a rotation about the $z-$ axis with a rotation angle $\theta = \frac{\pi}{4}$. Fig 5 c-d display the traces of the F and G in their $xy-$ planes. The 2-D projections of the image (5 c) with the view angles $\varphi = 0, \frac{\pi}{2}$ are shown in Fig 5e-f, and the projections of the image (5d) with the view angles $\varphi = 0, \frac{\pi}{2}$ are shown in Fig 5g-h. The angle θ is simply the shift in the cosine functions of (40), shown in Fig 5i.

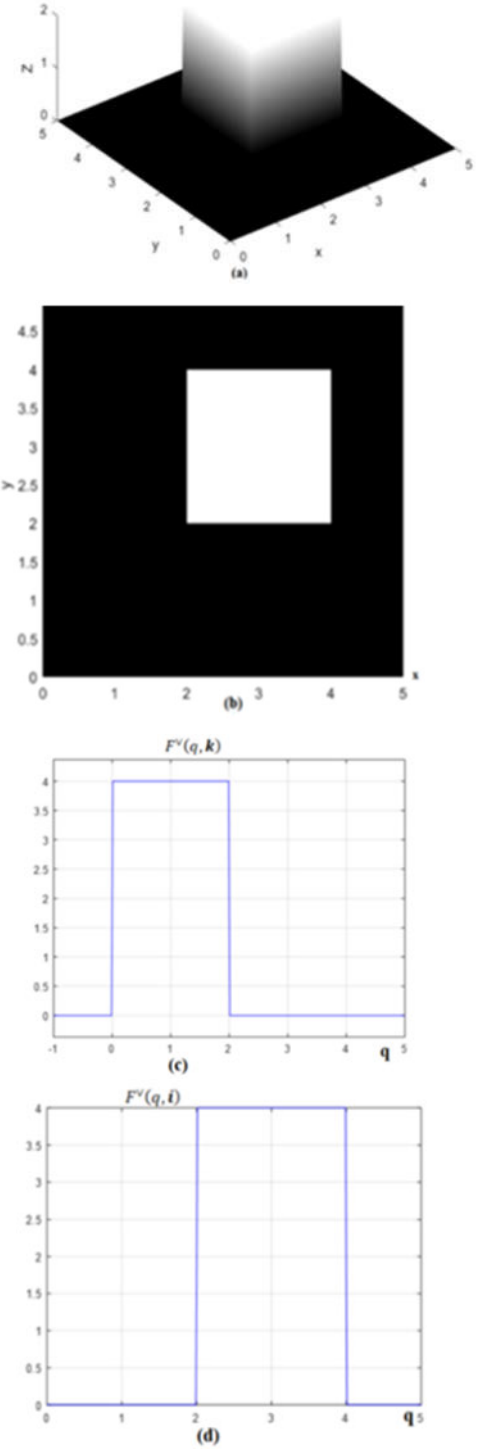

FIGURE 2. (a) Region E= {(x,y,z): 2 ≤ x ≤ 4, 2 ≤ y≤ 4,and 0 ≤ z ≤2 } on which F(x,y,z) = 1. (b) A horizontal slice of F shown on the xy- plane. (c). The profile $F^{\vee}(\boldsymbol{q}, \boldsymbol{k})$. (d) The profile $F^{\vee}(\boldsymbol{q}, \boldsymbol{i})$.

Further, let us solve this problem using two known methods. First, we apply the R-Signature [17], on the pair of images in Fig 5c-d. The R-transform or signature of $f^{\vee}(p, \varphi)$

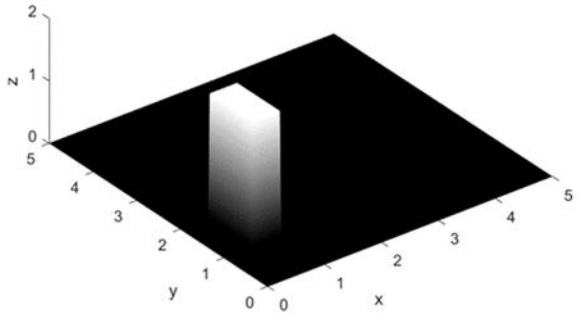

FIGURE 3. A scaled form G of F given by G(x,y,z) = F(4x,2y,1z).

is defined as

$$\mathcal{R}f^{\vee}(\varphi) = \int_{-\infty}^{\infty} [f^{\vee}(p,\varphi)]^2 \, dp \tag{47}$$

so that a rotation of the image by an angle θ implies a translation of the R-transform by θ. The R-transform signatures of images 5c-d are shown in Fig 5j, of which the shift equals $\frac{\pi}{4}$. Second, we apply the method of [6]. Let g be a rotation of f with angle of rotation θ. To recover the angle of rotation; [6] minimizes the function.

$$A(\theta) = \int_{\varphi=0}^{\pi} \int_{p=-\infty}^{\infty} |f^{\vee}(p, \varphi - \theta.) - g^{\vee}(p,\varphi)\ |^2 dp d\varphi. \tag{48}$$

A plot of $A(\theta)$ is shown in Fig 5k, of which the minimum occurs at $\theta = \frac{\pi}{4}$. The advantage of our current approach is building the two graphs appear in Fig 5i using only two view angles, $\varphi = 0, \frac{\pi}{2}$.

C. EXAMPLE 3: A 3-D ROTATION ABOUT AN ARBITRARY AXIS WITH ARBITRARY ANGLE OF ROTATION

Consider the function $F(x, y, z) = 1$ on the region $E = \{(x, y, z) : 0 \le x \le \frac{1}{2},\ 0 \le y \le \frac{1}{2}, 0 \le z \le 1\}$ shown in Fig 6a. Image G in Fig 6b is obtained from F by a rotation about the $z-$ axis with a rotation angle $\theta = \frac{\pi}{2}$. In this way, the support of F is in the first octant while the support of G is in the fourth octant. Traces of F and G in their $xy-$ planes are shown in Fig 6c-d, respectively. In other words, consider (42)-(46): we have

$$\boldsymbol{u} = \ <0, 0, 1>, \quad \theta = \frac{\pi}{2},$$
$$A_{\boldsymbol{u},\theta} = \begin{bmatrix} 0 & -1 & 0 \\ 1 & 0 & 0 \\ 0 & 0 & 1 \end{bmatrix},$$
$$G(x, y, z) := F\left[A_{\boldsymbol{u},\theta}\boldsymbol{x}\right],$$

and

$$G^{\vee}(q, \xi) = F^{\vee}(q, A_{\boldsymbol{u},\theta}\xi)$$

To minimize (46), consider the discrete form:

$$\Psi(\boldsymbol{u}, \theta) = \sum_{\boldsymbol{\xi}} \sum_{q} \left|G^{\vee}(q, \boldsymbol{\xi}) - F^{\vee}\left(q, A_{\boldsymbol{u},\theta}\xi\right)\right| \tag{49}$$

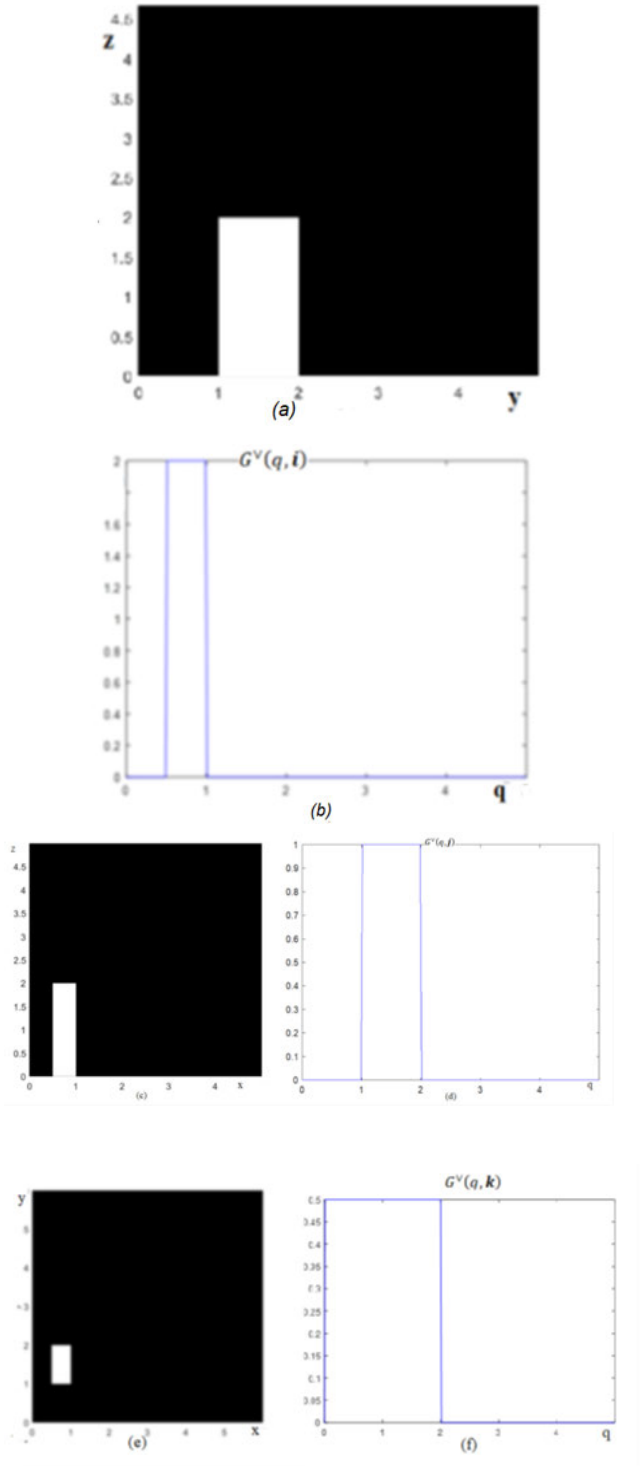

FIGURE 4. (a-b) A slices of Fig 3 parallel to the *yz*- plane together with the profile $G^{\vee}(q, i)$. (c-d) A slices of Fig 3 parallel to the xz plane together with the profile $G^{\vee}(q, j)$ (e-f) a slices of Fig 3 parallel to the *xy*- plane with the profile $G^{\vee}(q, k)$.

on some grids of the regions (44) and (45) and values of q. We used 317 possible vectors $\boldsymbol{u}$ from the upper half of the sphere (44), and 21 possible

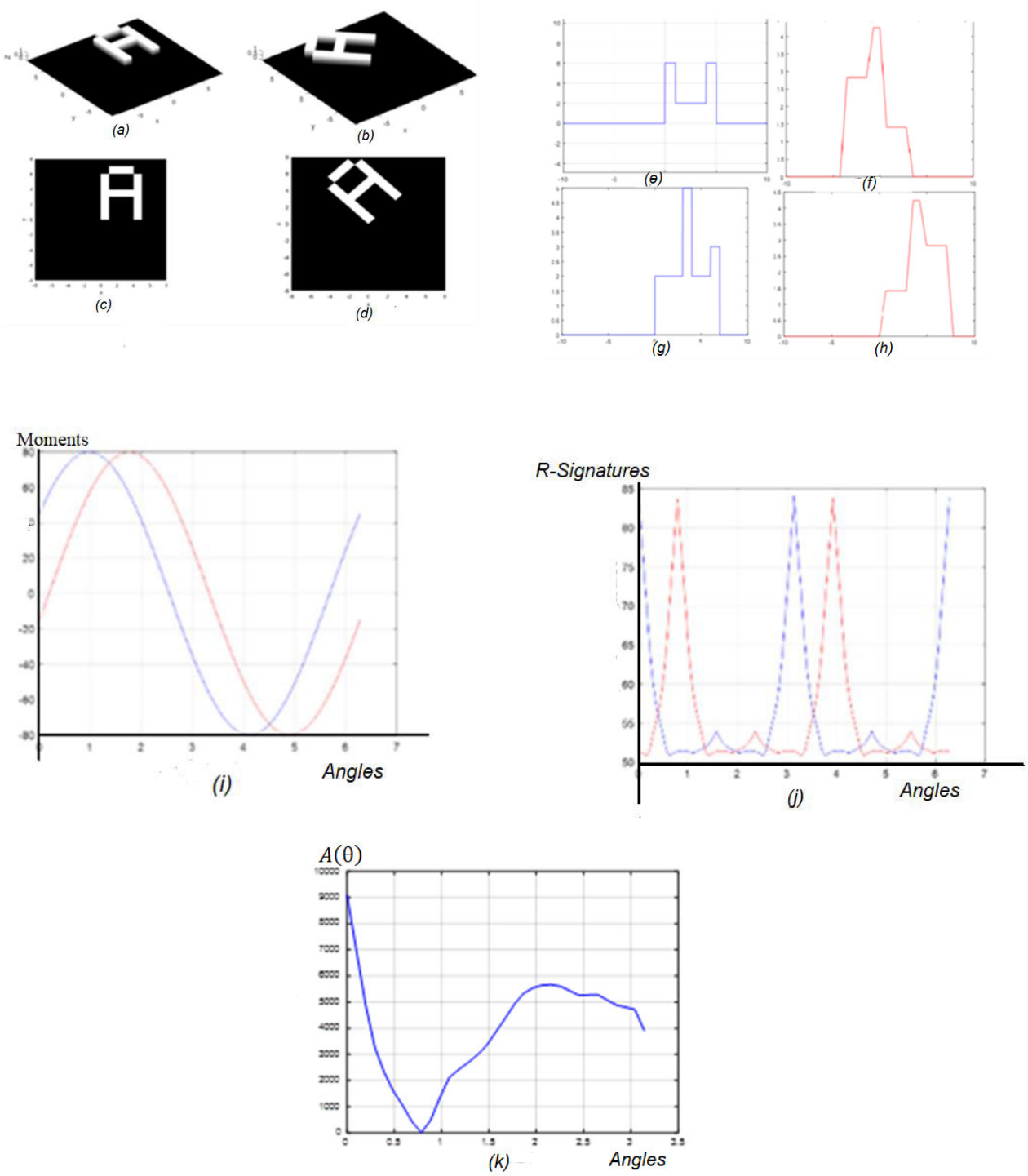

FIGURE 5. (a) original image, (b) G obtained from F by a rotation about the z- axis with a rotation angle $=\pi/4$. (c-d) traces of the F and G in their xy- planes. (e-f) The 2-D projections of the image (5c) with the view angles $\varphi = 0, \pi/2$. (g-h) the projections of the image (5d) with the view angles $\varphi = 0, \pi/2$. (i) Graphs of both sides of equation (40). (j) The R-signatures (47) of images 5c-d. (k) A(θ) from (48) of which the minimum occurs at $\theta = \pi/4$.

values of θ. In this way, there are 6657 evaluations of $\Psi(\boldsymbol{u}, \theta)$ from (49). Finer choices of these variables and parameters are, of course, possible. For a visual display, we show a one-dimensional plot for the values of $\Psi(\boldsymbol{u}, \theta)$ against the sequential order of iterations,as shown in Fig 6e. From Fig 6e, at the 1744^{th}

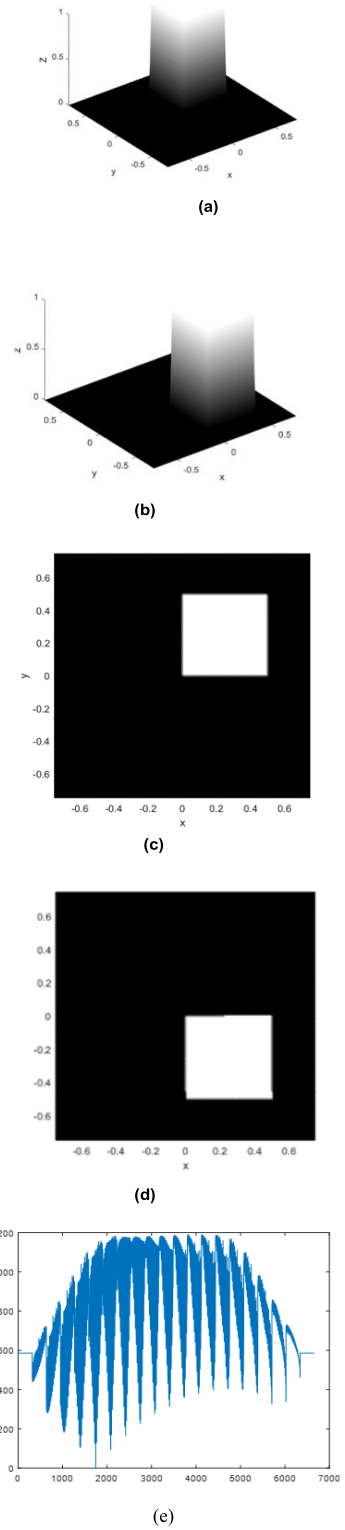

FIGURE 6. (a) original image, (b) G obtained from F by a rotation about the z- axis with a rotation angle $\theta = \pi/2$. (c-d) traces of F and G in their xy- planes. (e) one dimensional plot for the values of $\Psi(u,\theta)$ against the sequential order of iterations from (49).

iteration, the minimizers are $\boldsymbol{u} =< 0, 0, 1 >$ and $\theta = \frac{\pi}{2}$. Observe that if vectors $\boldsymbol{u}$ were chosen from the lower half of the sphere, then the minimizers would be $=< 0, 0, -1 >$ and $\theta = \frac{3\pi}{2}$.

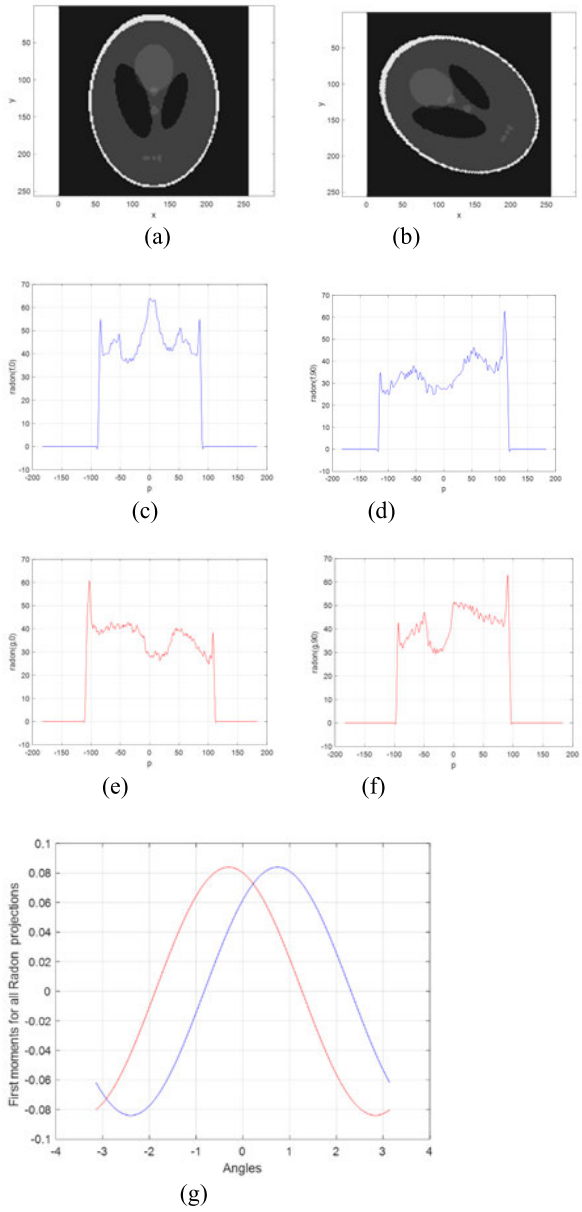

FIGURE 7. (a) original image f, (b) g obtained from f by a rotation with a rotation angle $\theta = \pi/3$. (c-d) projections of f with view angles $\varphi = 0, \pi/2$. (e-f) the projections of g with view angles $\varphi = 0, \pi/2$. (g) Graphs of both sides of equation (40).

D. EXAMPLE 4: A 2-D ROTATION

In our last example, we consider a Shepp–Logan phantom f, of size 256×256. This image is shown in Fig 7a, its rotation g with $\theta = \pi/3$ is shown in Fig 7b. In Fig 7c-d, we display the projections of f with view angles $\varphi = 0, \pi/2$.

In Fig 7e-f, we display the projections of g with view angles $\varphi = 0, \pi/2$. And, the graphs of both sides of

equation (40) are shown in Fig 7g, of which the shift equals $\pi/3$.

V. CONCLUSION

We have seen that this work improved the results of [6] and [7]. In [6], the problems of shifting, rotating, reflecting, dilating, and translating between a reference image and a distorted image were addressed. In [7], the general form of the problem is solved by recovering the singular value decomposition of the matrix. This work introduced the following improvements:

1) A solution to the 2-D non-uniform scaling problem.
2) An alternative solution to the 2-D rotation problem using only two orthogonal projections such as the view angles 0 and $\pi/2$.
3) Computing the centroid and scaling parameters in the 3-D setting by reducing the 3-D to 2-D calculations.
4) An efficient method of recovering a rotation of a 3-D image around an arbitrary axis and an angle of rotation.

REFERENCES

[1] J. Modersitzki, *FAIR: Flexible Algorithms for Image Registration*. Philadelphia, PA, USA: Society for Industrial and Applied Mathematics, 2009.

[2] S. Paul and U. C. Pati, "A comprehensive review on remote sensing image registration," *Int. J. Remote Sens.*, vol. 42, no. 14, pp. 5396–5432, Jul. 2021.

[3] W. Cao, "Applying image registration algorithm combined with CNN model to video image stitching," *J. Supercomput.*, vol. 77, no. 12, pp. 13879–13896, Dec. 2021.

[4] J. Jose, N. Gautam, M. Tiwari, T. Tiwari, A. Suresh, V. Sundararaj, and M. Rejeesh, "An image quality enhancement scheme employing adolescent identity search algorithm in the NSST domain for multimodal medical image fusion," *Biomed. Signal Process. Control*, vol. 66, Apr. 2021, Art. no. 102480.

[5] H. Kim, H. Cho, and C. Oh, "Rotation estimation and segmentation for patterned image vision inspection," *Electronics*, vol. 10, no. 23, p. 3040, 2021.

[6] F. Hjouj and D. W. Kammler, "Identification of reflected, scaled, translated, and rotated objects from their radon projections," *IEEE Trans. Image Process.*, vol. 17, no. 3, pp. 301–310, Mar. 2008, doi: 10.1109/TIP.2007.916160.

[7] F. Hjouj and M. S. Jouini, "On the radon transform and linear transformations of images," in *Proc. DMIP*, Shanghai, China, Nov. 2019, pp. 26–31, doi: 10.1145/3379299.3379306.

[8] F. I. Hjouj and M. Soufiane Jouini, "On image registration using the radon transform: Review-and-improvement," in *Proc. DMIP*, Kyoto, Japan, Nov. 2021, pp. 17–23, doi: 10.1145/3506651.3506654.

[9] L. Arrowood, "Projection registration applied to nondestructive testing," *J. Electron. Imag.*, vol. 19, no. 3, Jul. 2010, Art. no. 031208.

[10] Y. Wan and N. Wei, "A fast algorithm for recognizing translated, rotated, reflected, and scaled objects from only their projections," *IEEE Signal Process. Lett.*, vol. 17, no. 1, pp. 71–74, Jan. 2010.

[11] T. Fujisawa and M. Ikehara, "High-accuracy image rotation and scale estimation using radon transform and sub-pixel shift estimation," *IEEE Access*, vol. 7, pp. 22719–22728, 2019, doi: 10.1109/ACCESS.2019.2899390.

[12] H. S. Kim and H.-K. Lee, "Invariant image watermark using Zernike moments," *IEEE Trans. Circuits Syst. Video Technol.*, vol. 13, no. 8, pp. 766–775, Aug. 2003.

[13] A. Venkataramana and P. A. Raj, "Image watermarking using Krawtchouk moments," in *Proc. Int. Conf. Computing: Theory Appl. (ICCTA)*, Mar. 2007, pp. 676–680.

[14] D. Zhang and G. Lu, "Shape-based image retrieval using generic Fourier descriptor," *Signal Process., Image Commun.*, vol. 17, no. 10, pp. 825–848, Nov. 2002.

[15] H. Zhu, M. Liu, and Y. Li, "The RST invariant digital image watermarking using radon transforms and complex moments," *Digit. Signal Process.*, vol. 20, no. 6, pp. 1612–1628, Dec. 2010.

[16] G. Y. Chen, T. D. Bui, and A. Krzyżak, "Invariant pattern recognition using radon, dual-tree complex wavelet and Fourier transforms," *Pattern Recognit.*, vol. 42, no. 9, pp. 2013–2019, Sep. 2009.

[17] T. V. Hoang and S. Tabbone, "The generalization of the R-transform for invariant pattern representation," *Pattern Recognit.*, vol. 45, no. 6, pp. 2145–2163, Jun. 2012.

[18] B. Xiao, J.-F. Ma, and J.-T. Cui, "Combined blur, translation, scale and rotation invariant image recognition by radon and pseudo-Fourier–Mellin transforms," *Pattern Recognit.*, vol. 45, no. 1, pp. 314–321, Jan. 2012.

[19] K. Zhan, J. Teng, and Y. Ma, "Spiking cortical model for rotation and scale invariant texture retrieval," *J. Inf. Hiding Multimedia Signal Process.*, vol. 4, pp. 155–165, Jul. 2013.

[20] D. L. Rizzini, "Angular radon spectrum for rotation estimation," *Pattern Recognit.*, vol. 84, pp. 182–196, Dec. 2018.

[21] H. Sasaki, K. Kobayashi, T. Aoki, M. Kawamata, and T. Higuchi, "Rotation measurements using rotation invariant phase only correlation," *ITE Tech. Rep.*, vol. 22, no. 45, pp. 55–60, Sep. 1998.

[22] S. Nagashima, K. Ito, T. Aoki, H. Ishii, and K. Kobayashi, "A high-accuracy rotation estimation algorithm based on 1D phase-only correlation," in *Proc. Int. Conf. Image Anal. Recognit. (ICIAR)*, M. Kamel and A. Campilho, Eds. Berlin, Germany: Springer, 2007, pp. 210–221, doi: 10.1007/978-3-540-74260-9_19.

[23] H. Bay, A. Ess, T. Tuytelaars, and L. Van Gool, "Speeded-up robust features (SURF)," *Comput. Vis. Image Understand.*, vol. 110, no. 3, pp. 346–359, 2008.

[24] S. Leutenegger, M. Chli, and R. Y. Siegwart, "BRISK: Binary robust invariant scalable keypoints," in *Proc. Int. Conf. Comput. Vis.*, Barcelona, Spain, Nov. 2011, pp. 2548–2555, doi: 10.1109/ICCV.2011.6126542.

[25] P. Markelj, D. Tomaževič, B. Likar, and F. Pernuš, "A review of 3D/2D registration methods for image-guided interventions," *Med. Image Anal.*, vol. 16, no. 3, pp. 642–661, 2012.

[26] Z. Špiclin, B. Likar, and F. Pernuš, "Fast and robust 3D to 2D image registration by backprojection of gradient covariances," in *Biomedical Image Registration*, vol. 8545, S. Ourselin and M. Modat, Eds. Cham, Switzerland: Springer, 2014, doi: 10.1007/978-3-319-08554-8_13.

[27] Y. Jiangsheng, L. Weiguo, L. Jian, G. Gene, and L. Zhengrong, "Image matching for translation, rotation and uniform scaling by the Radon transform," in *Proc. Int. Conf. Image Process. (ICIP)*, vol. 1, Chicago, IL, USA, 1998, pp. 847–851, doi: 10.1109/ICIP.1998.723649.

[28] A. Lange and S. Heldmann, "Multilevel 2D–3D intensity-based image registration," in *Biomedical Image Registration* (Lecture Notes in Computer Science), vol. 12120, Ž. Špiclin, J. McClelland, J. Kybic, and O. Goksel, Eds. Cham, Switzerland: Springer, 2020, doi: 10.1007/978-3-030-50120-4_6.

[29] S. Liu, B. Yang, Y. Wang, J. Tian, L. Yin, and W. Zheng, "2D/3D multimode medical image registration based on normalized cross-correlation," *Appl. Sci.*, vol. 12, no. 6, p. 2828, Mar. 2022.

[30] J. Radon, "On the determination of functions from their integral values along certain manifolds," *IEEE Trans. Med. Imag.*, vol. MI-5, no. 4, pp. 170–176, Dec. 1986, doi: 10.1109/TMI.1986.4307775.

[31] S. R. Deans, *The Radon Transform and Some of Its Applications*. New York, NY, USA: Wiley, 1983.

[32] F. Hjouj, "Towards tomography with random orientation," in *Proc. DMIP*, Shanghai, China, Nov. 2019, pp. 49–53, doi: 10.1145/3379299.3379309.

[33] M. S. Jouini, F. Bouchaala, M. K. Riahi, M. Sassi, H. Abderrahmane, and F. Hjouj, "Multifractal analysis of reservoir rock samples using 3D X-ray micro computed tomography images," *IEEE Access*, vol. 10, pp. 67898–67909, 2022, doi: 10.1109/ACCESS.2022.3186476.

[34] M. S. Jouini, F. Bouchaala, E. Ibrahim, and F. Hjouj, "Permeability and porosity upscaling method using machine learning and digital rock physics," in *Proc. 83rd EAGE Annu. Conf. Exhib.* Noida, India: EAGE, 2022, pp. 1–5, doi: 10.3997/2214-4609.202210016.

[35] G. N. Hounsfield, "Computerized transverse axial scanning (tomography): Part 1. Description of system," *Brit. J. Radiol.*, vol. 46, no. 552, pp. 1016–1022, Dec. 1973, doi: 10.1259/0007-1285-46-552-1016.

[36] C. L. Epstein, *Introduction to the Mathematics of Medical Imaging*. Upper Saddle River, NJ, USA: Pearson, 2003.
[37] F. Hjouj and M. S. Jouini, "Computed tomography reconstruction using only one projection angle," *IEEE Access*, vol. 11, pp. 9672–9679, 2023, doi: 10.1109/ACCESS.2023.3239956.
[38] T. J. Wang and T. W. Sze, "The image moment method for the limited range CT image reconstruction and pattern recognition," *Pattern Recognit.*, vol. 34, no. 11, pp. 2145–2154, Nov. 2001.

FAWAZ HJOUJ received the Ph.D. degree in mathematics from Southern Illinois University, USA, in 2004. He was an Assistant Professor with the Mathematics Department, East Carolina University, USA. In 2013, he joined the Petroleum Institute, United Arab Emirates, which became a part of Khalifa University. He has active research on radon transformation that synthesizes numerical analysis and Fourier analysis, which includes computations on digital image processing with applications to different problems in the field of computerized tomography.

MOHAMED SOUFIANE JOUINI received the master's degree in electrical engineering, the M.Sc. degree in signal and image processing from the National Polytechnic Institute of Toulouse, and the Ph.D. degree in signal and image processing from Bordeaux University. He held several positions with research and development centers in the industry before joining academia. He was a Research Scientist in digital rock physics with TOTAL E&P Research Center, PAU, France, from 2006 to 2009. Then, he was appointed as a Research and Development Engineer in image processing algorithms for security applications with SAGEM SECURITE (IDEMIA) Research and Development Center, Paris, France. In January 2010, he joined ADNOC (Petroleum Institute) as a Research and Teaching Associate to work on projects in digital rock physics. In 2014, he was appointed as an Assistant Professor with the Mathematics Department, Khalifa University. He is currently an Associate Professor of mathematics, experienced in numerical simulations to model rock properties based on X-ray computed tomography images.

MOHAMMAD AL-KHALEEL received the M.Sc. and Ph.D. degrees in applied mathematics (numerical analysis and scientific computing) from McGill University, Montreal, QC, Canada, in 2003 and 2007, respectively. In 2007, he became an Assistant Professor of mathematics with the Department of Mathematics, Yarmouk University, Jordan, and was promoted to Associate Professor. He is currently an Associate Professor with the Department of Mathematics, Khalifa University, United Arab Emirates. His research is multidisciplinary but the bulk of it has revolved around developing and implementing efficient and parallel numerical methods as well as analytical methods for solving differential equations (ordinary, partial, and fractional) that appear in many applications in different fields, including seismic waves, nanofluid and microfluid dynamics, circuit simulations, and many others. His research interests include mathematics, including topics in metric fixed point theory, fractional calculus, numerical parameter optimization, inverse and control problems, and the mathematical background of computer arithmetic circuits.